Chapter 4

Molecular Mechanism of Interaction of Curcumin with BSA, Surfactants and Live E. Coli Cell Membrane Revealed by Fluorescence Spectroscopy and Confocal Microscopy†

†This work has been published. "Molecular Mechanism of Interaction of Curcumin with BSA, Surfactants and Live *E. Coli* Cell Membrane Revealed by Fluorescence Spectroscopy and Confocal Microscopy" ***Pratibha Agarwala****, Turban Bera, Dr. Dibyendu K. Sasmal* ChemPhysChem* **2022**, *23*,18,e202200265

In this chapter, we discuss our work on mechanism of interaction of curcumin with bovine serum albumin (BSA) and live *E. coli* cell membrane in the presence of organized assemblies of sodium dodecyl sulfate (SDS) and cetrimonium bromide (CTAB) by fluorescence spectroscopy, laser-scanning confocal microscopy, and computation.

4.1 Introduction

Protein–surfactant interactions have been extensively studied due to their various applications in daily life (detergents, cosmetics, foods, and pharmaceuticals) using various techniques including ultrafast fluorescence spectroscopy, scattering based spectroscopy, mass spectroscopy, microscopy and computation.[168-176] The formation of micelles spontaneously increases the entropy of the system and minimizes the formation of unfavorable hydrocarbon-water contacts, often called the hydrophobic effect. The interaction study of globular protein with surfactant creates a mechanism of understanding how surfactant behaves as a denaturant and solubilizing agent for protein and lipid vesicles.[177-180] The ionic surfactant strongly interacts with protein, and generally denatures them at low concentrations, whereas non-ionic surfactants are usually not expected to denature.[181-182] Protein unfolding is caused by the initial interactions between the surfactant and protein, where the protein is exposed to more binding sites.[20, 183] Serum albumin proteins are the major soluble plasma proteins with many physiological functions such as transport, distribution, and metabolism of ligands that act as carrier proteins. BSA is a globular protein (M.W. is 66.5 kDa) comprised of 583 amino acids, 17 disulfide bonds and a free cysteine group with three homologous α-helical proteins at least six binding sites available for binding.[184] There are number of studies on effect of curcumin in cells and animals, but its low biocompatibility and low solubility have decreased its applications as medicine, and therefore increasing the solubility is a major topic of research that will ultimately benefit the research on clinical trials.[185] Pascalau et al. has reported a method on delivery of curcumin through BSA/polysaccharides multi-layered microcapsules. They used CaCO3 template to synthesize non-toxic CaCO3/BSA particles as micro-templates that contains BSA, and then they made BSA gel to load with curcumin.[186] However, the significant drawback with protein is that it can undergo various physical changes or structural instability such as aggregation at pH value close to isoelectric point, thermal denaturation etc. The utilization of surfactants is beneficial in the drug and vaccine delivery system.[47, 187] Their aggregation behaviors are well defined, and a hydrophobic drug solution stabilized by micelles can be easily produced at the industry level. However, the main problem arises when the surfactant loses its micelle structure due to low concentration and become insoluble.[188] A molecular understanding of the interaction of curcumin with a combination of BSA and surfactants may give a potential direction for development of drug delivery system at physiological conditions. Although the significance of curcumin as a drug has been clearly understood and used for centuries, the lack of understanding of molecular

mechanism of interaction and solvation of curcumin with protein, made it challenging to use as therapeutics. The contradictory nature of low solubility and high binding affinity with protein is also poorly understood.

Here, we report our findings for understanding the molecular mechanism of interaction of low soluble curcumin with BSA, SDS (CMC = 0.008 mol L^{-1})[189], and CTAB (CMC = 0.0009 mol L^{-1})[190], and live bacteria cell membrane. We have studied, the photophysical properties of curcumin bound to BSA in the presence of surfactant and explained in detail on binding, using spectroscopic methods such as steady-state absorption, fluorescence spectroscopy and confocal imaging of individual bacteria. To analyze the molecular interaction between curcumin and an extrinsic fluorescence probe Coumarin 102 (C102), we have used confocal microscopic imaging technique[191] in live bacteria where non-radiative (dipole-dipole) energy transfer is possible, when donor and acceptor are situated at distances of less than 10 nm.[146, 192]

4.2 Methods

4.2.1 Sample Preparation

Preparation of BSA solution: The protein solutions are prepared in tris-buffer with a specified concentration at pH = 7.4 for all experiments. The concentrations of BSA solution is calculated from a UV-VIS spectrophotometer using a molecular absorption coefficient of ε = 43,800 M-1 cm^{-1} at 278 nm.[193]

Preparation of Curcumin solution: Curcumin stock solution is prepared in ethanol and concentrations are measured by determining optical density (OD) at the λ_{max} = 429 nm (using ε = 55,000 M^{-1} cm^{-1}).[194] Final curcumin solutions are made in Mili-Q water before experiments so that the ethanol concentration is less than 0.05%.

Preparation of C102 solution: The stock solution of C102 is made in ethanol. The stock solution concentration is calculated by determining the OD at λ_{max} = 389 nm by a spectrophotometer (using ε =2.15×104 M^{-1} cm^{-1}).[195] The working concentration of C102 is made in Mili-Q water in such a way that the ethanol concentration is less than 0.05 %.

All stock solutions of dye and protein are stored in the dark at 4°C.

4.2.2 UV-VIS Spectroscopy

UV–VIS absorption spectra of all samples are acquired on LabIndia-2000U spectrophotometer at room temperature with a quartz cuvette of path-length of 1 cm. Concentration of the protein, drug and dye solutions are determined spectrophotometrically for each solution before any experiments. Number of bacteria present in a solution is also calculated by UV-VIS spectroscopy as per described methods.[196]

4.2.3 Fluorescence Spectroscopy

The steady-state fluorescence spectra are measured in a JASCO FP-8300 spectrofluorimeter (Japan Spectroscopic Company) at room temperature using a quartz cuvette of path-length 1 cm. Curcumin is excited at λ_{ex} = 425 nm, and the emission spectra are scanned from λ_{em} = 450 to 600 nm with a slit of 2.5 nm; otherwise, it is specified. For BSA, BSA-SDS, BSA-CTAB, fluorescence spectra are measured at λ_{ex} = 279 nm and λ_{em} = 300 to 500 nm. The extrinsic probe C102 is excited at λ_{ex} = 389 nm, and emission data are collected from the λ_{em} = 405 nm to 650 nm. The excitation and emission slit are set at 2.5 nm.

For 3D-fluorescence spectroscopy measurements, an inbuilt program is used where a range of emission spectra are determined for a range of excitation wavelength with specific intervals for both excitation and emission. Then 3D intensity counter plots with color are determined based on their emission intensity range. This 3D emission spectra are usually specific for a molecular interaction based on their structure, conformation and reaction, and thus it is known as

fingerprint of a molecule. We have utilized this principle to understand the structure and conformational changes of BSA in the presence of surfactant and drug molecules.

4.2.4 Calculation of Binding Isotherm

The binding isotherm curve also explains the interaction between the protein–surfactant. Figure 4.1.F shows the binding isotherms by plotting the average number of surfactant (SDS/CTAB) bound per protein (BSA) (v) in BSA + Surfactant system vs the total concentration of surfactant used.[177] The following equation is used to calculate an average number of CTAB or SDS bound per protein (BSA),

$$v = \alpha \frac{[S]}{[P]} \tag{4.1}$$

Where fraction of surfactant bound to protein referred as α, the total concentration of surfactant and protein expressed as [S] and [P], respectively. In order to find out the fraction of surfactant bound to the protein the following equation is used,

$$\alpha = \frac{F_{obs} - F_{free}}{F_{sat} - F_{free}} \tag{4.2}$$

F_{obs} and F_{free} represented the intensity of Tryptophan (Trp) residue in the presence and absence of quencher, and F_{sat} is the intensity at saturated condition.

4.2.5 Circular Dichroism (CD) Spectroscopy

Circular dichroism spectra are measured by JASCO J-815 Spectrophotometer (Japan Spectroscopic Company) using a 2 mm quartz cuvette at room temperature. The spectra for all protein solutions are collected at 5 bar nitrogen pressure with a scan speed of 200 nm/min. from 180 nm to 400 nm with an interval of 0.1 nm. Blank measurements are performed for spectra correction before the measurement of protein samples.

4.2.6 *E. coli* Bacteria Culture

Gram-negative bacteria, *E. coli* (DH5α) is grown in LB-broth solution at 37 °C for 15 hours in a shaker incubator before measuring the number by OD measurement. The incubation of dye or drug is also performed in shaker incubator after thoroughly washing bacteria in Mili-Q water. This strain is stored at -80 °C in 50 % glycerol solution until they are sub-cultured for further studies. For microscopy, cells are cultured overnight in LB broth and washed three times with Mili-Q water before being strained with fluorescent dye. Then, cells are incubated for 2 hours in 0.23 mM of C102, 0.76 mM of curcumin, and in a mixture solution of 0.23 mM of C102 and 0.76 mM of curcumin. Cells are washed three times, immobilized between cover glass (0.17 mm thickness) and glass slide, and used for microscopy study within 10 min.

4.2.7 Laser Scanning Confocal Microscopy for FRET Imaging

Olympus FV1000 laser scanning confocal microscope is used for FRET imaging to understand molecular interaction in live bacteria cell membrane at room temperature. To do that, a solid-state CW-laser of 405 nm with peak power of 25 mW is passed through AOTF and single-mode fiber-optics, focused on sample through 1X tube lens and 100X (1.40 NA) oil immersion objective via a confocal scanning mirror. The fluorescence signal is passed through laser clean-up filter followed by grating before detection by PMT connected photo-diode in analog-mode.

For FRET imaging on bacteria cell surface, donor (C102) and acceptor (Curcumin) fluorescence signals are separated by dichroic mirror (DM405/488), collected by two PMT

channels in scanning mode where each channel (Donor + Acceptor) are selected by grating with a resolution of 2 nm. Collected images are analyzed by ImageJ and OriginPro.

4.2.8 Calculation of FRET Efficiency

According to Förster's theory, the energy transfer efficiency (E) is dependent on the inverse of sixth power of intermolecular distance, as per following equation:[21, 131]

$$E = \frac{R_0^6}{R_0^6 + r^6} \quad (4.3)$$

Where 'r' is the distance between the donor and acceptor at which 50% of the excitation energy is transmitted from donor to the acceptor and R_0 is called Förster's distance, evaluated by the equation:

$$R_0 = [8.79 \times 10^{-25} \kappa^2 n^{-4} \Phi J(\lambda)]^{1/6} \quad (4.4)$$

Where the orientation factor denoted as κ^2, varies from 0 to 2, for liquid solutions $\kappa^2 = 2/3$, refractive index of the solution, n = 1.333 (for water) in the present case. Φ expressed as quantum yield of the donor (C102), Φ = 0.76 here.[197] J(λ) is denoted the product of the spectral overlap integral between the normalized donor fluorescence spectra and acceptor excitation spectra as

$$J(\lambda) = \frac{\int_0^\infty F(\lambda) .\varepsilon(\lambda). \lambda^4 d\lambda}{\int_0^\infty F(\lambda). d\lambda} \quad (4.5)$$

Where F(λ) indicates normalized donor intensity at the wavelength λ, ε(λ) indicates the acceptor molar absorption coefficient at λ. For our study, we have prepared 0.5 µM sol. of C102 and 34.87 µM sol. of curcumin; the concentration is measured from absorbance as mentioned earlier. Experimentally found that $J(\lambda) = 1.178 \times 10^{15}$ M^{-1} cm^{-1} nm^4 with 89% energy transfer efficiency (Figure 4.14.A). The values of R_0 and r are 6.8 nm and 4.79 nm respectively evaluated using Equations 4.3 and 4.4. The average value of r i.e., donor to acceptor distance is 5 nm, which lies in the range of $0.5\ R_0 < r < 1.5\ R_0$ indicates that the energy transfer and interaction from C102 to curcumin are possible.

We also explored the possibility of fluorescence resonance energy transfer (FRET) from donor to acceptor directly in living cells. The acceptor (C102) strained bacterial presence in the presence and absence of donor (Curcumin) is excited with 405 nm laser and under constant condition measurements.

The FRET calculation is done by using[190]

$$E = \frac{I_{A(D)}^{corr}}{I_{A(D)}^{corr} + I_{(D)}^{corr}} \quad (4.6)$$

Where $I_{A(D)}^{corr}$ is corrected acceptor intensity in presence of donor, and $I_{(D)}^{corr}$ is corrected donor intensity in absence of acceptor, measures in the presence of both dyes. Bleed-through from donor and acceptor is calculated to be 3.28 and 5.28 respectively.

4.2.9 Computational Details

All theoretical calculations have been carried out using the Gaussian16 quantum chemical package. Geometries of all structures involved in this study are optimized and characterized using hybrid exchange-correlation functional B3LYP[198] together with Pople's 6-31G++(d,p)[199] basis set without any constraints double-ζ split valence basis set for all the atoms in the solvent

phase. The solvent effect is characterized using water as solvent (ε = 78.4) by Conductor-like Polarizable Continuum Model (CPCM).[200-201]

4.2.10 Molecular Docking Analysis

Molecular docking analysis is carried out utilizing AutoDock Tools 4.2 to calculate the binding affinity and energies of ligand (curcumin) bind to protein (BSA). The 3D crystal structure of the protein BSA (PDB 3V03) is downloaded from the protein data bank (www.rcsb.org). The ligand used for the current study is accessed from NCBI PubChem (https://pubchem.ncbi.nlm.nih.gov/) database. For the conversion of SMILE format of ligand into the .pdb format, the Open Babel software is used.[202]

The modified structure of protein and ligand is used in AutoDock Tools, and the Gasteiger partial charge procedure is used to calculate partial charges of atoms.[203] Autodock tools are used to merge nonpolar hydrogen of protein and ligand. Also, the atomic charge and rotatable bonds are assigned to a ligand. The grid map of dimension 114×108×112 is applied, and grid spacing of 0.603 Å is used to include the protein's binding sites. Using AutoDock Tools, all the parameter files such as grid and docking parameter are set up. All other default parameter settings were used.[204] At the end, Docking calculations are carried out using Lamarckian genetic algorithm[205] with the rigid modified protein and a flexible ligand. Finally, from the output file of the docking, the most stable energy is implemented as the most favourable structure of the BSA-curcumin complex. All the post-screening analysis of the docked complex is done using BIOVIA Discovery Studio.

4.3 Results & Discussion

4.3.1 Partial Unfolding of BSA by Surfactants Revealed by Fluorescence Quenching and CD Spectroscopy

First, we studied intrinsic fluorescence spectra of BSA (Figure 4.1.A) from λem = 300 nm to 500 nm upon λex = 279 nm at room temperature in the presence of anionic surfactant (SDS) and cationic surfactant (CTAB), as illustrated in Figure 4.1.(B-C) respectively. It is observed that native BSA exhibited an emission maximum at λ_{em}^{max} = 346.5 nm because of two Tryptophan (Trp) amino acid residues present in the protein. The addition of surfactant often quenched its intrinsic fluorescence approximately 4-times depending upon the concentration, possibly because of collision quenching. Notably, the change in $\Delta\lambda_{em}^{max}$ of 24 nm (CTAB, black line) and 31 nm (SDS, red line) concerning different concentrations of surfactant is also evident from Figure 4.1.D. Upon addition of 0.2 mM SDS/CTAB into 50 µM BSA, there is almost no change in emission maxima of BSA, but the fluorescence intensity is decreased because of low molecular ratio Surfactants:BSA = 4:1. However, the sharp change in Trp fluorescence intensity, as well as blue shifted λ_{em}^{max} is observed when Surfactants:BSA molecular ratio is increased from 4:1 to 800:1, indicating that the Trps are exposed to a more hydrophobic environment compared to the bulk polar water environment. The structural changes in native BSA arise due to the surfactant-assisted unfolding of the tertiary structure of protein caused by electrostatic and hydrophobic interactions.[179-180, 206] This result shows micelles may form around the protein backbone, providing a nonpolar hydrophobic micro-environment to the Trp molecule. Similar unfolding nature of Human Serum Albumin is also reported when treated with SDS.[179, 206] The area under the curve (Figure 4.1.B) shows a similar decrease with increasing the SDS concentration from 0.5 to 10 mM. The steps of binding of SDS/CTAB to native BSA is non-cooperative in nature, and the breaking point exemplifies this aggregation in the graph. Increasing the concentration of SDS/CTAB above 10 mM to 40 mM in BSA, indicates the interactive nature of surfactants. The added surfactant molecules show almost no binding affinity toward BSA as the emission, and fluorescence intensity shift is more or less unchanged beyond the molecular ratio of 200:1. The diffusion

coefficient of native BSA is 6 x 10^7 cm^2/s[207], and the addition of surfactants 800-times molecular ratio to the number of native BSA not only causes the structural collapse and decrease in diffusion but also partial recoiling around the micelle, which is clearly evident from sharp change of λ_{em}^{max}. In addition, the estimated α helix and β sheet in native BSA are 56.8% and 5.8% respectively,[208] and addition of surfactants of either positive or negative headgroup will be absorbed inside protein microenvironment depending on preference or interplay between electrostatic and hydrophobic interactions.

Our results in Figure 4 align with previous fluorescence-based investigations of protein-surfactant interactions, including those conducted by Moriyama et al.[209] and De et al.[177] Moriyama et al. attributed the fluorescence quenching of serum albumin by SDS to structural alterations and enhanced solvent exposure of Trp residues owing to protein unfolding. This aligns with our discovery of a notable blue shift (~24–31 nm) in BSA fluorescence emission with the addition of SDS and CTAB, suggesting the relocation of Trp residues to a more hydrophobic milieu. Their research, while concentrating on binding constants and denaturation thresholds, failed to quantify alterations in secondary structure or present comprehensive binding isotherms—components we elaborate on through CD spectroscopy and thermodynamic modeling.

In the study conducted by De et al.[177] , the researchers employed fluorescence spectroscopy to investigate the interaction between human serum albumin (HSA) and SDS. They identified three separate binding regions: initial specific binding, cooperative micelle binding, and saturation, as indicated by Stern-Volmer and modified Scatchard studies. In our study, we find three binding areas (A–C) for both SDS and CTAB by Stern-Volmer and binding isotherm studies.

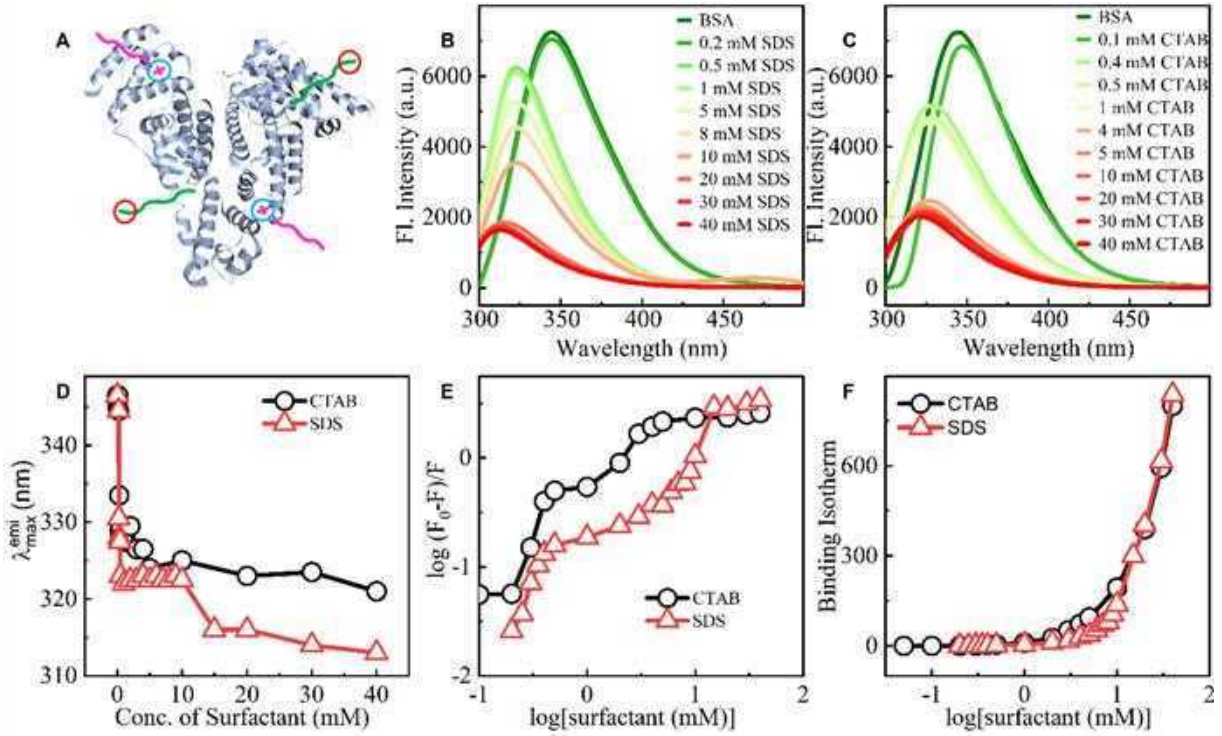


Figure 4.1 (A) Schematic representation of protein BSA (PDB ID: 3v03) surfactant interaction. Cationic and anionic surfactants are represented in different colors. (B) Fluorescence emission spectra of BSA (50 μM) excited at 279 nm without (top green line) and with SDS from 0.2 mM to 40 mM concentration at pH = 7.4. (C) Fluorescence emission spectra of BSA (50 μM) excited at 279 nm without (top green line) and with CTAB from 0.2 mM to 40 mM concentration at pH = 7.4. (D) Variation of emission maxima (nm) of BSA in the presence of surfactants CTAB (black) and SDS (red) at various concentrations. (E) The plot of log (F_0-F)/F vs. log[surfactant]

as per Stern-Volmer equation. (F) The observed changes in binding isotherm of BSA in the presence of surfactants.

The CD spectra are typically characterized by two negative peaks due to n → π* transition at 208 nm and 222 nm. Our CD spectroscopy study of BSA with various concentrations of SDS and CTAB (Figure 4.4) clearly shows (increase of peaks at 208 nm and 222 nm) the partial denaturation of tertiary structure of native BSA at room temperature due to disruption of S-S bonds as well as hydrogen bonds. We have calculated the mean residual ellipticity (MRE) value by the following equation:[210]

$$\text{MRE} = \frac{\text{observed CD (mdeg)}}{c_p \times l \times n \times 10} \quad (4.7)$$

where, Cp is the molar concentration of protein, l = path length of cuvette (1 cm). n = number of amino acid residues (583 in BSA).
The α-helix is calculated as,

$$\alpha \text{ helix percentage} = \frac{(-\text{MRE}_{222} - 3000) \times 100}{33000} \quad (4.8)$$

The α-helix is calculated to be decreased from 58% to 49% for addition of 10 mM SDS, and 58% to 47% for addition of CTAB which clearly shows a loss in helicity due to the surfactants.

Quenching of fluorescence is the process where the quantum yield of fluorophore is decreased, induced by various molecular interactions such as, (i) excited state reactions, (ii) energy transfer, (iii) complex formation in the ground state and (iv) collisional quenching.[211] The mechanism of quenching for intrinsic fluorescence of native BSA with surfactants is a dynamic process and studied according to the Stern-Volmer equation as below.[208]

$$\frac{F_0}{F} = 1 + K_{sv}[Q] \quad (4.9)$$

Where relative intensity of fluorescence of BSA in the absence and presence of quencher are represented by F_0 and F respectively, K_{sv} is expressed as the Stern-Volmer quenching constant and quencher concentration is denoted by [Q]. Stern-Volmer plot is again divided into three different parts depending on the slope of curve, and corresponding quenching constant of each region is summarized in Table 4.1. The following modified Stern-Vomer equation is used to evaluate the binding constant, K and number of binding sites, n:

$$\log[F_0 - F]/F = \log K + n\log[Q] \quad (4.10)$$

From Figure 4.1.E, the plot of log [(F_0-F)/F] vs log[Q], it is assumed that the binding of surfactants SDS/CTAB to BSA takes place in different stages as marked by regions A-C (See Figure (4.1- 4.2) and Table 4.1). Using Equation 4.10, the values of K and n are calculated and summarized in Table 4.1. The Stern-Volmer plot in Figure 4.1.E is divided into three regions (Figure 4.1- 4.2) based on slope of curves - region A (<0.3 mM CTAB), where no shift in emission maxima is observed, region B (0.4-5 mM CTAB), where protein started to feel hydrophobic environment, region C (5-40 mM) where saturation occurs. Interestingly, the quenching constant is decreased by more than 100 times and the number of binding sites are decreased by 97 times whereas the binding constants remained unchanged from region A to region C.

The association constant for CTAB in Table 4.1, region B (above CMC of CTAB = 0.0009 mol L^{-1}) is 2.19 $Lmol^{-1}$, whereas for region A (below CMC) is 2.64 $Lmol^{-1}$ which conclude that in the micellar region, the binding affinity is higher. Above the micelle concentration, the CTAB form aggregation among themselves lowering the binding affinity. But in region C, the binding constant is slightly higher, the most likely explanation is upon surfactant binding the protein-

surfactants assembly swells in size, which allows more number of available binding sites. Similarly, graph for SDS is divided into three regions (Figure 4.1- 4.2), region A (0.2 to 0.4 mm), where the binding isotherm increases moderately due to specific ionic binding between surfactant and protein. Region B (0.5-10 mM of SDS), where the protein feels more hydrophobic environment at the CMC of SDS (CMS of SDS = 0.008mol L^{-1}), illustrates non-cooperative binding, where there is a steep rise beyond the CMC of SDS, and region C, where the binding curve almost gets saturated (15-40 mM of SDS).

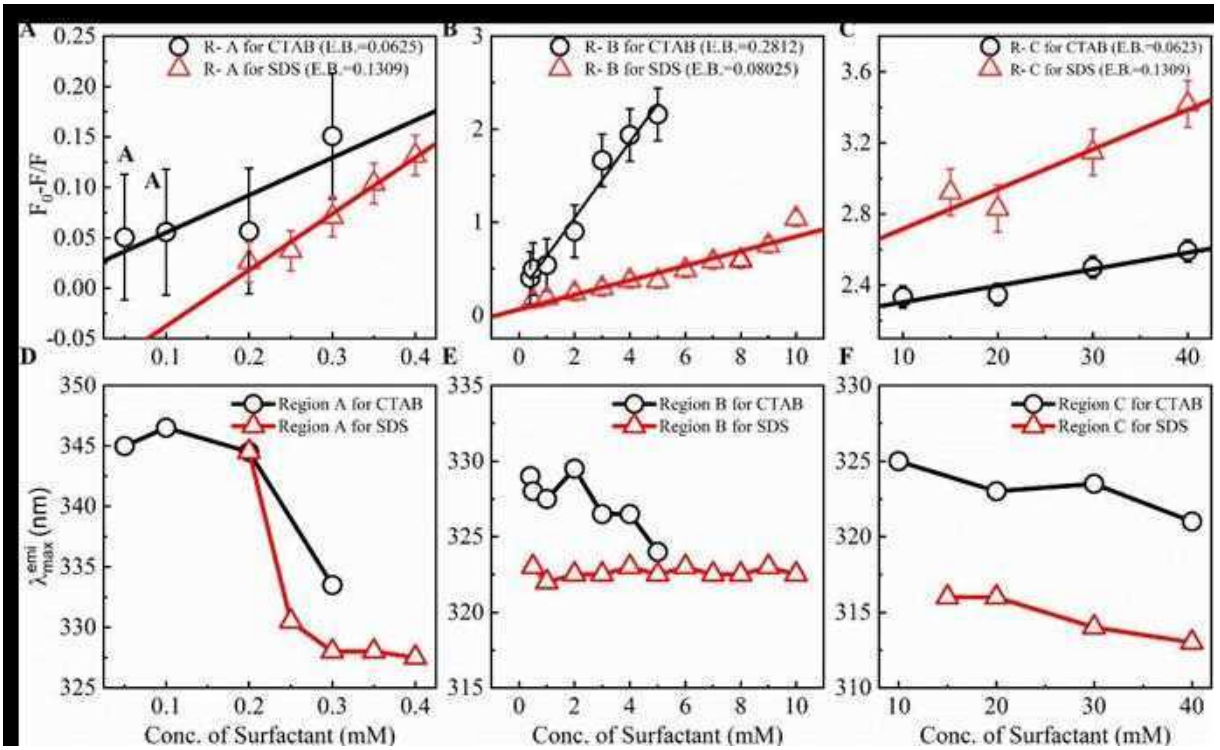


Figure 4.2 (A-C) Plot of (F_0-F)/F vs concentration of surfactant as per Stern-Volmer equation. The region (A-C) black line represents the binding stage of BSA in presence of CTAB & red line indicates the binding stage of BSA in presence of SDS, as illustrated. (D-F) The observed changes in emission maxima vs concentration of surfactant are represented in figure (D-F).

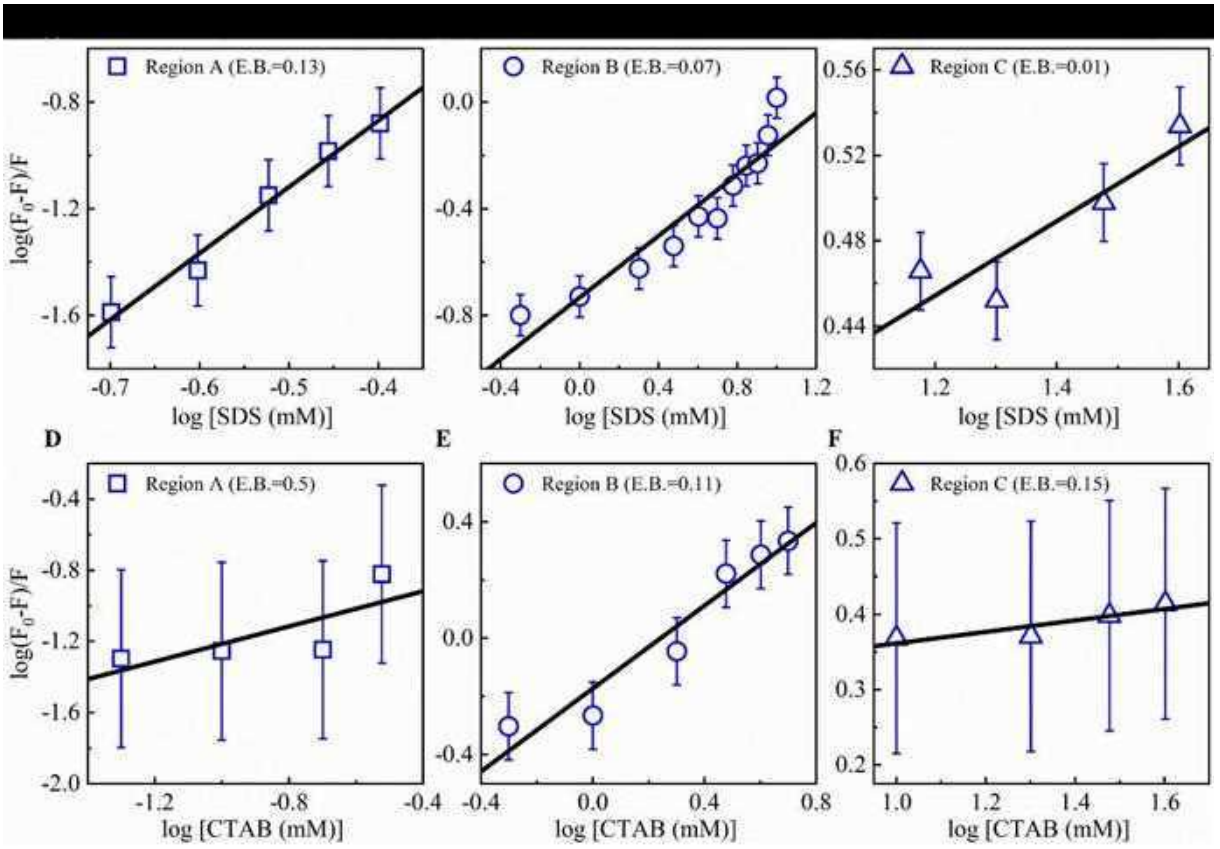


Figure 4.3 (A-C) The plot of log $(F_0-F)/F$ vs log [Surfactant] as per modified Stern-Volmer equation. The region (A-C) black line represents the binding stage of BSA in the presence of SDS. The region (A-C) black line represents BSA's binding stage in the presence of CTAB in figure (D-F).

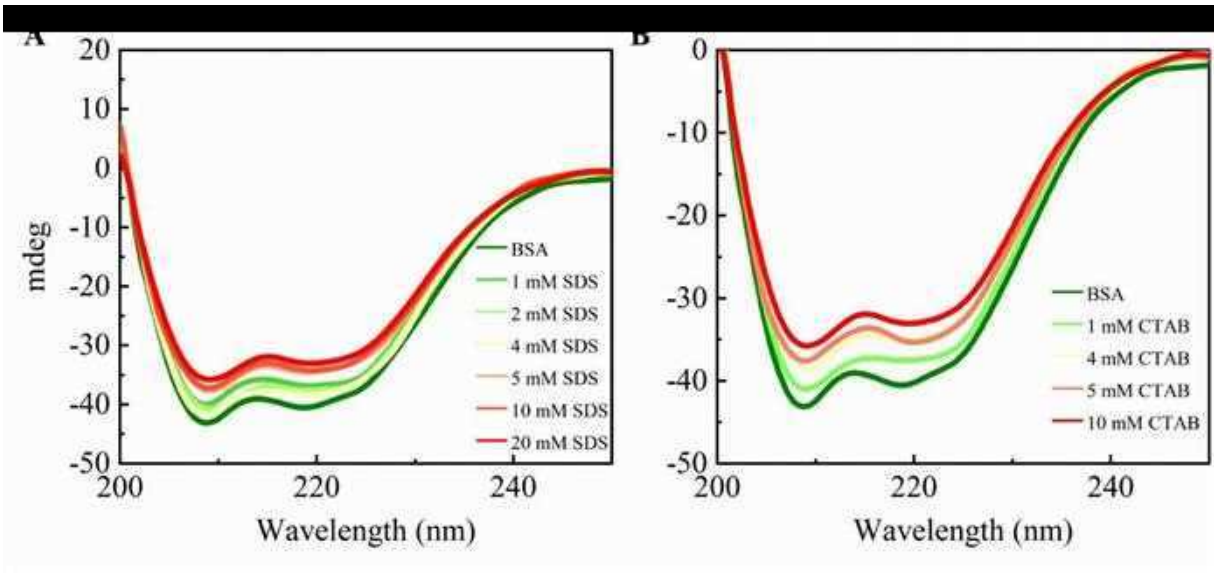


Figure 4.4 (A) The plot represents Far-UV CD spectra of BSA without and with different concentrations of SDS from 1 mM to 20 mM at pH 7.4 and 25 °C. (B) Far-UV CD spectra of BSA without and with different concentration of CTAB from 1 mM to 10 mM at pH 7.4 and 25 °C.

Calculation of binding isotherms (details in Experimental Section Equation 4.1, Figure 4.1.F and Figure 4.3.(G-I)) also displayed the characteristic region as (A) specific binding, (B) non-cooperative binding (C) saturation. The region A described the specific binding pattern for SDS

and CTAB. In this region, the binding isotherm rises slowly due to specific ionic binding between surfactant and protein. Region B represents non-cooperative binding, where the rise is gradual. The region C reveal the saturation point where earlier surfactant binding to protein has caused partial uncoiling of native protein structure (Figure 4.3.(G-I)).

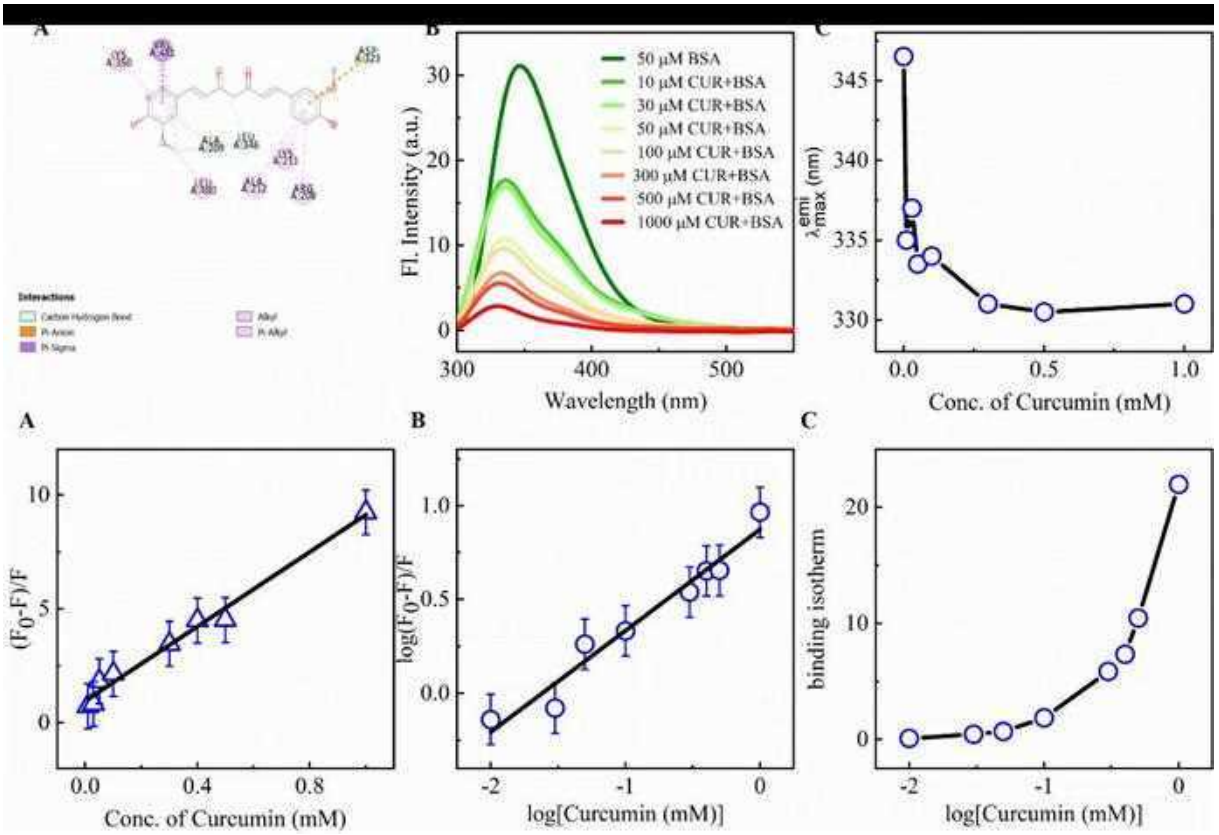


Figure 4.5 (A) 2D pictorial presentation of drug (curcumin) protein BSA (PDB Id: 3v03) interaction. (B) Emission spectra of BSA (50 µM) excited at 279 nm in absence and presence of different concentrations of curcumin from 0.01 mM to 1 mM at pH= 7.4 (C) Variation of emission maximum (nm) of BSA (50 µM) excited at 279 nm in absence and presence of different concentrations of curcumin from 0.01 mM to 1 mM at pH= 7.4 (D) Plot of $(F_0\text{-}F)/F$ vs concentration of curcumin (E) plot of log $(F_0\text{-}F)/F$ vs log[surfactant] as per Stern-Volmer equation (F) The observed changes in binding isotherm of BSA in presence of curcumin.

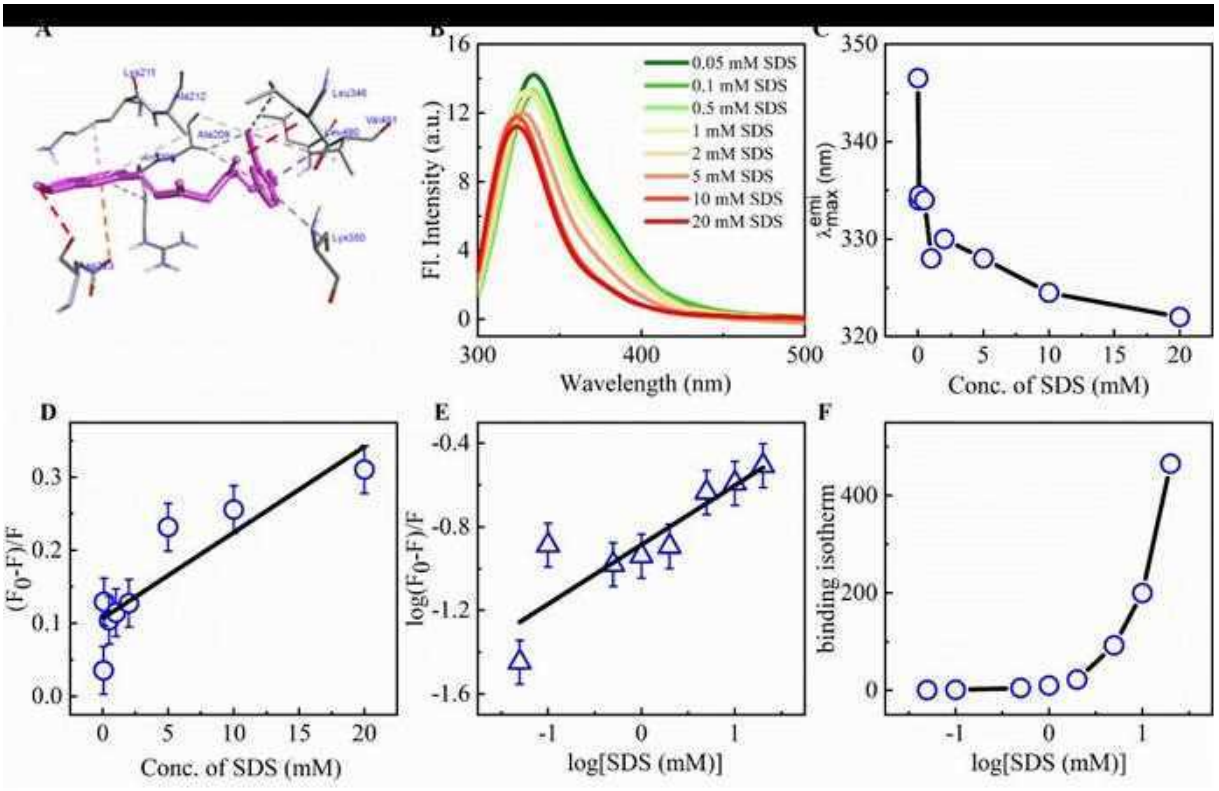


Figure 4.6 (A) 3D representation showing docking of curcumin with the active site of BSA. The dashed red line represents the hydrogen bond. The ligand is represented in the magenta color. (B) Emission spectra of mixture of BSA (50 µM) and curcumin (50 µM) excited at 279 nm in presence of different concentrations of SDS from 0.05 mM to 20 mM at pH = 7.4. (C) Variation of emission maxima of mixture of BSA and curcumin in presence SDS. (D) Plot of $(F_0\text{-}F)/F$ vs concentration of SDS. (E) Plot of log $(F_0\text{-}F)/F$ vs log[SDS] as per Stern-Volmer equation. (F) The observed changes in binding isotherm of mixture of BSA and curcumin in presence of SDS.

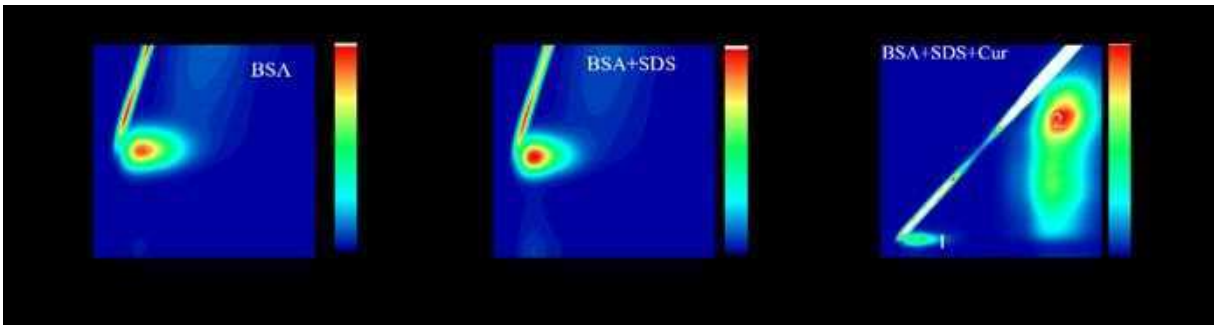


Figure 4.7 3D fluorescence analysis of 50 µM BSA (A), 50 µM BSA + 10 mM SDS (B) and 50 µM BSA + 50 µM Curcumin + 10 mM SDS (C).

4.3.2 Mechanism of Interaction Between Curcumin and BSA in Presence of Surfactants

Computations and spectroscopy studies are used to detect the binding of a small molecule such as a drug to protein by monitoring the binding energy and shift in emission maxima. Molecular docking analysis using AutoDock Tools 4.2 (details in Experimental Section) showed

that curcumin in protein environment has binding energy -6.1 kcal-mol^{-1}, which is energetically favorable. The post-screening analysis shows the formation of hydrogen bonds between amino acid LYS 211 and LEU 480 of chain-A with curcumin at bond lengths 3.37 Å and 2 Å, respectively (Table 4.3, Figure 4.5.A). The 2D interaction profile also showed that it stabilizes through convention hydrogen, alkyl and pi-alkyl bonding, as depicted in Figure 4.6.A and Table 4.3. Hydrogen bonding plays a crucial role in stabilizing the protein-ligand complex, and other forces like van der Waals and hydrophobic force help in stabilizing the nonpolar ligand too.

Fluorescence spectroscopy is used to investigate the interaction of curcumin with BSA because fluorescence intensity and emission maxima are highly sensitive to the molecular interactions. The interaction of curcumin with BSA is expressed by the following equation:

$$nCur + BSA = [nCur : BSA] \quad (4.11)$$

where n is the number of curcumin molecules. Curcumin has low solubility in bulk water, and at λ_{ex} = 425 nm, curcumin exhibits weak fluorescence at 572 nm in aqueous solution, the interaction between curcumin and protein can be identified by the fluorescence quenching, which is dynamic in nature. It is observed that with increasing the concentration of curcumin, fluorescence intensity emitted by BSA is reduced (Figure 4.5.B). The emission maximum is shifted 15 nm from 346.5 nm (emission maxima of pure BSA) to 331 nm due to the binding of the aryl group of curcumin to the less polar cavity of BSA (Figure 4.5.C). The influence of curcumin on BSA fluorescence emission is shown in Figure 4.5 - 4.6 For 50 µM curcumin with 50 µM BSA alone, the emission maximum is 335.5 nm; after adding 10 mM SDS to the of BSA + curcumin complex, it is shifted to 324.5 nm (Figure 4.6.(B-C)). This result may be ascribed due to the electrostatic interaction arises between the cationic patches (i.e., -NH_3^+) of amino acids present on native BSA and anionic sulfate head groups (i.e., -SO_4^-) of SDS. This outcome suggests that in presence of curcumin more bathochromic shift is observed in BSA-SDS complexes than that of BSA alone, which faciles the loading of curcumin into hydrophobic core. To determine the quenching mechanism, we assumed that the interaction belongs to dynamic quenching and analyzed by Stern–Volmer equation as described in Equation 4.9. The quenching constant and the binding isotherm plot are illustrated in the Figure 4.5.(D-F) and Figure 4.6.(D-F).

The changes of intrinsic fluorescence intensity and emission maxima of BSA can be utilized to understand the molecular mechanism of binding of BSA and BSA-SDS complexes in presence of curcumin. As illustrated in Figure 4.7.(A-B), the emission maxima of BSA in three-dimensional fluorescence spectroscopy is observed at 342 nm at excitation at 300 nm. A hypochromic shift of BSA towards the less polar environment is observed after successive addition of curcumin into BSA solution. Tryptophan 213 (Trp-213) residue in the hydrophobic cavity of BSA is mainly liable for the intrinsic fluorescence intensity of BSA.[212] Considering the hydrophobic nature of curcumin, it is anticipated that the curcumin access to the hydrophobic pockets close to Trp-213 group, results in the hypochromic shift in fluorescence intensity of BSA. The peak 1 in Figure 4.7.C represents the BSA fluorescence spectra at emission maxima 330 nm. The peak 2 represents the curcumin emission spectra, showing a broad spectrum with emission maxima at 582 nm.

The steady increase in the concentration of SDS from 0.01 mM to 20 mM to the constant concentration of BSA + Curcumin complex (50 µM BSA + 50 µM curcumin) decreases the intensity of BSA (Figure 4.6.B). This result suggests that the aggregation of SDS inside the BSA+ curcumin complex is favorable to quench the fluorescence of Trp residue in BSA. Consequently, curcumin can easily penetrate the hydrophobic cavity of protein due to unfolding caused by anionic surfactant than that of only protein. This outcome suggests a possibility of energy transfer from donor Trp-213 of BSA to acceptor curcumin, which is enhanced in the presence of anionic surfactant. The binding constant (K) of curcumin in presence of only BSA and assembly of BSA-SDS have been calculated by Equation 4.10 in Table 4.2. The representative fluorescence intensity changes of BSA in the presence of different curcumin concentrations are shown in Figure 4.5. The higher value of binding constant K = 2.94 M^{-1} of curcumin for the BSA + SDS system, than curcumin with BSA alone (2.87 M^{-1}) indicates a higher affinity for curcumin with BSA-SDS

complex. It was also shown that at λ_{ex} = 425 nm (Figure 4.8), curcumin shows two peaks in the fluorescence spectra due to keto-enol tautomerism, one at 491 nm due to enol form, another one is at 536 nm due to the keto form, with increasing the concentration of SDS, there is a 4 nm hydrophobic shift due to the solubilization in the micellar core.

We want to highlight the point here that in the presence of SDS, the number of binding sites is decreased almost 47%, and also the quenching constant also decreased 99.85 fold (Table 4.1). The probable reason of the minimal impact of SDS in BSA + Curcumin system may be the hydrophobic curcumin are captured in the micelle core, and the interaction between BSA and SDS is decreased, which is also evident from 50% decrease of number of binding sites in case of SDS in BSA + Curcumin mixture (Table 4.2).

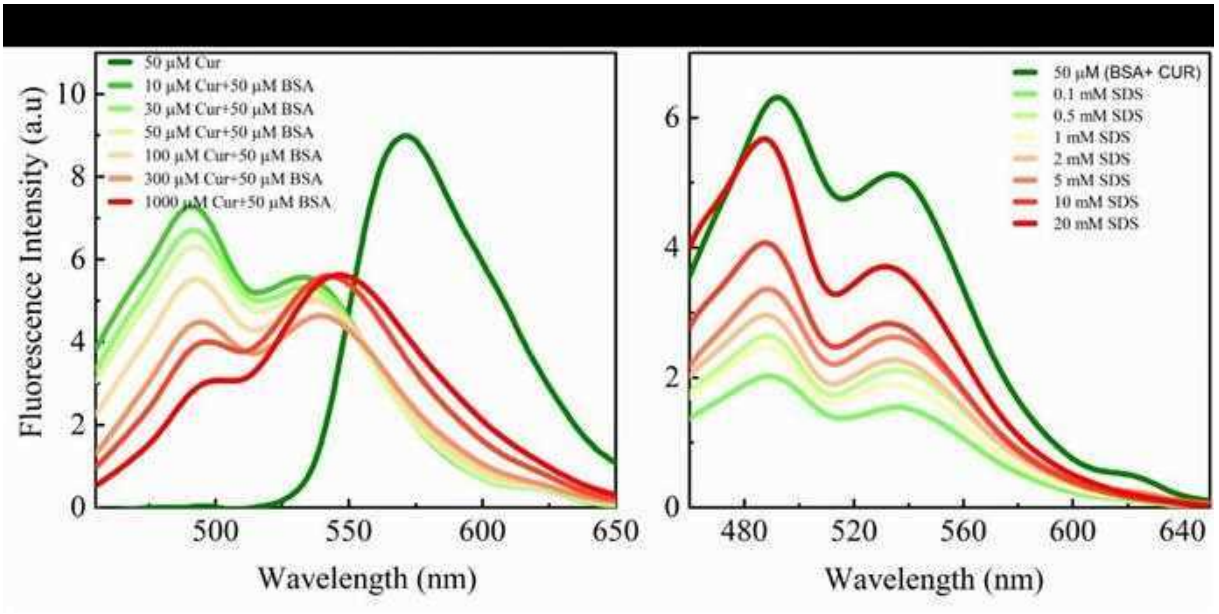


Figure 4.8 (A) Normalized fluorescence spectra of different concentrations of curcumin from 0.01 mM to 1 mM in absence and presence of BSA (50 µM) excited at 425 nm at pH = 7.4. (B) Normalized fluorescence spectra of mixture of BSA (50 µM) and curcumin (50 µM) excited at 425 nm in the presence of different concentrations of SDS from 0.1 mM to 20 mM at pH = 7.4.

4.3.3 Cat-anionic mixed micelle disfavours partial unfolding of proteins

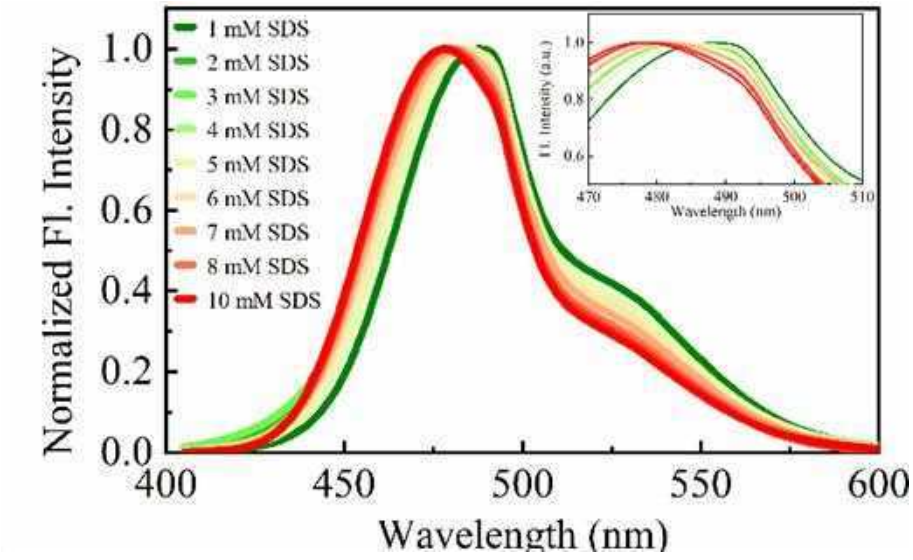


Figure 4.9 Normalized fluorescence spectra of 0.2 mM CTAB in presence of 1 mM to 10 mM SDS concentrations. The inset shows a representative plot corresponding to emission maxima changes.

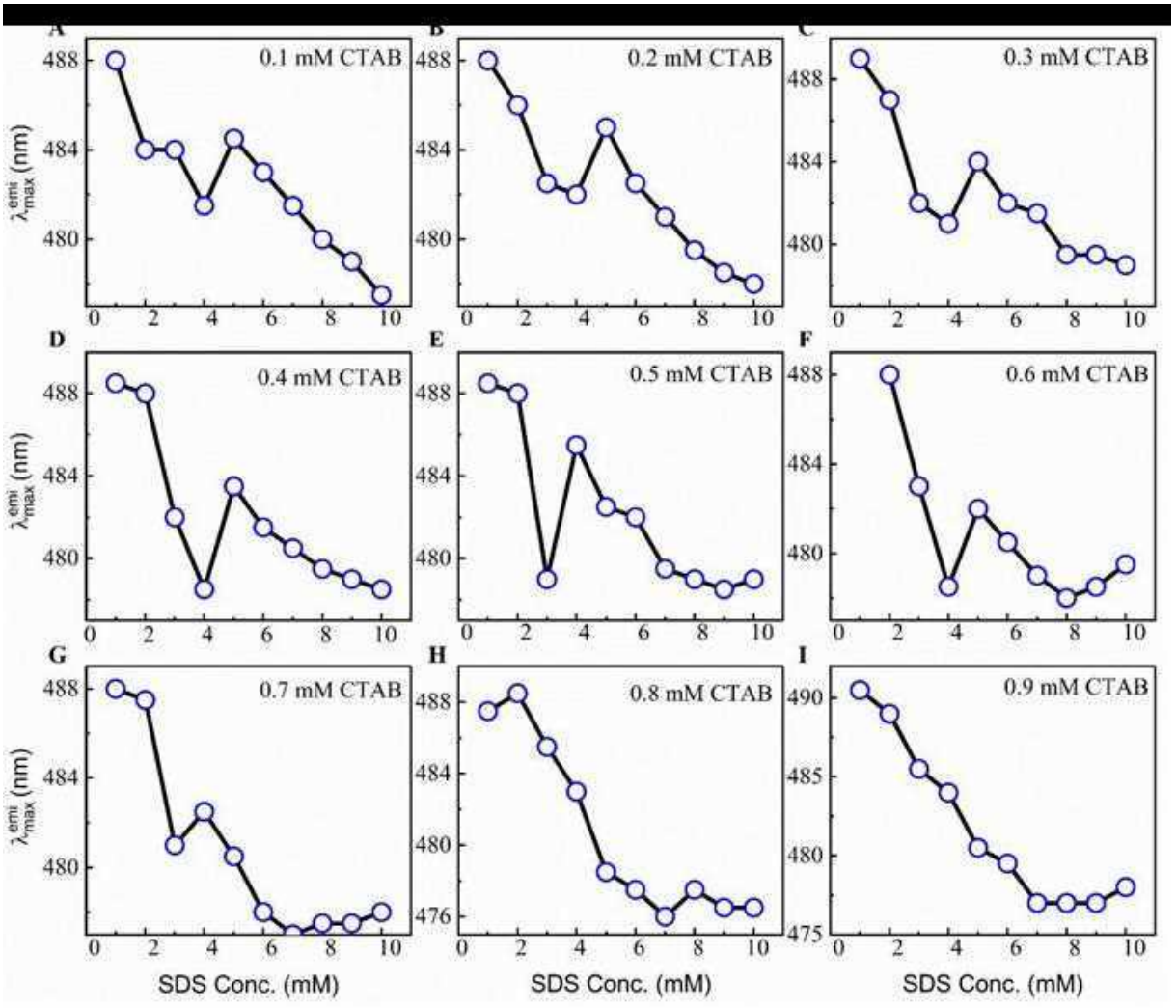


Figure 4.10 Plot of emission maxima changes of C102 probe in mixed micelle system at constant CTAB concentrations with change in SDS concentration.

An indication of polarity inside the mixed micelle is obtained from the fluorescence emission of C102 with a mixture of CTAB and SDS. We studied the system 0.2 mM CTAB in the presence of 1-9 mM of SDS (Figure 4.9). The plot of emission maxima (nm) vs surfactant concentration (Figure 4.10) shows a profile that the C102 passes to a more hydrophobic environment as the concentration of surfactant increases. Our investigation reveals that mixed micelle facilitates the presence of monomeric surfactants with higher hydrophobicity. In other words, we can predict that the higher amount of surfactant in the mixed micelles assembly (Figure 4.10) of monomeric cat-anionic surfactant leads to a reduction of CMC values in the mixed micelle. The interaction of BSA with the mixture of cationic-anionic surfactant is also investigated by fluorescence spectroscopy (Figure 4.11). However, the change of emission maxima with the cat-anionic surfactant mixture is not as probable as the cationic or anionic surfactants itself. For the equimolar mixture of different concentrations of the cat-anionic mixture (from 0.05 mM to 5 mM), the emission maxima change 10 nm in the hydrophobic region (Blue-shift, Figure 4.11. (A-B)).

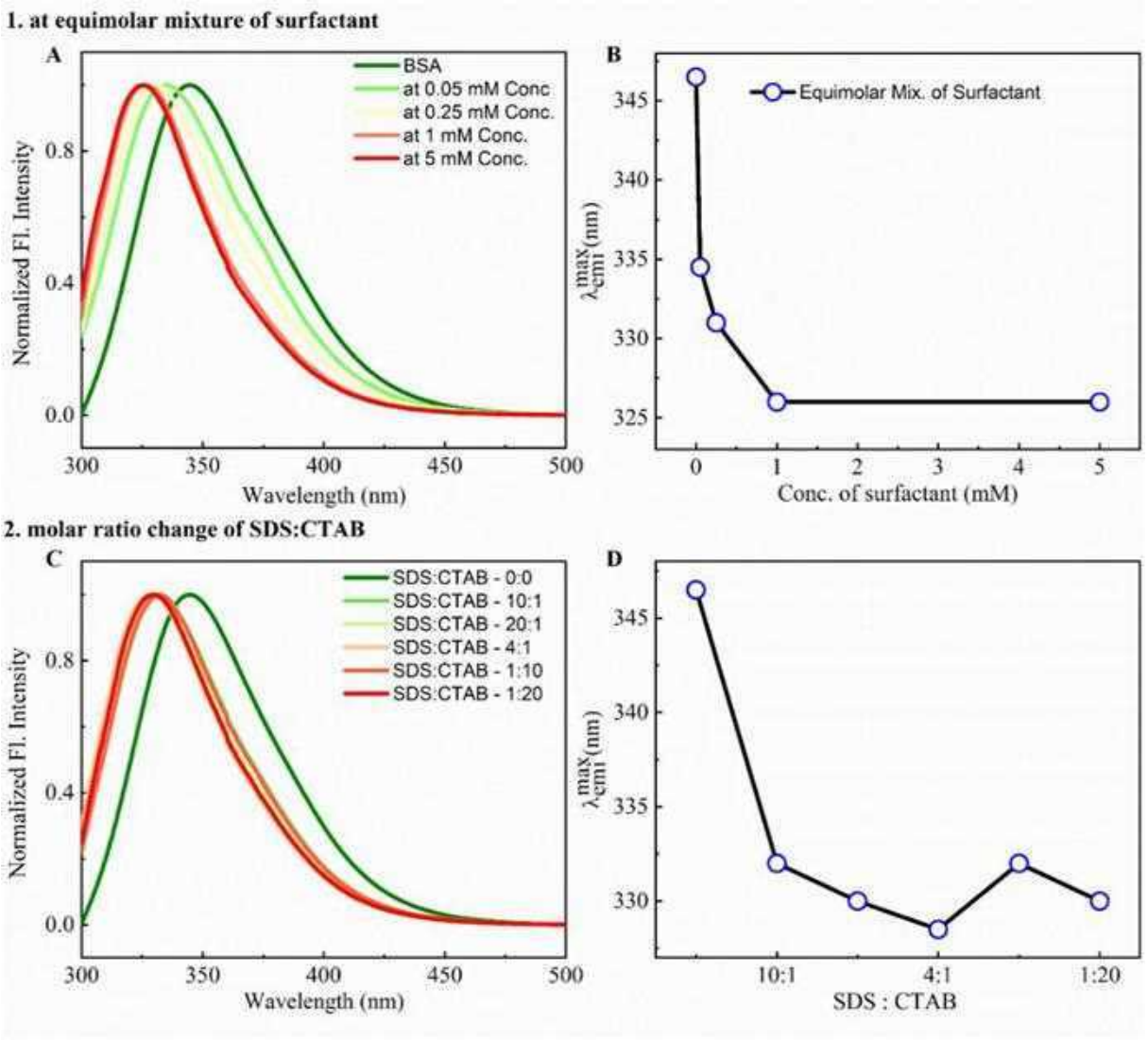


Figure 4.11 1(A) Normalized spectra of fluorescence intensity of BSA (50 µM) excited at 279 nm without and with an equimolar mixture of surfactants (SDS & CTAB) from 0.05 mM to 5 mM at pH = 7.4, (B) A representative plot of corresponding fluorescence emission spectra plot of BSA (50 µM) vs the concentration of surfactants (SDS & CTAB) for an equimolar mixture. 2(A) Normalized spectra of fluorescence intensity of BSA (50 µM) excited at 279 nm without and with surfactants (SDS & CTAB) at different molar concentrations at pH = 7.4, (B) A representative plot of fluorescence emission spectra of BSA (50 µM) vs the concentration of surfactants (SDS & CTAB).

Regarding molar ratio change (below CMC), we have checked for SDS: CTAB from 1:1 to 1:20 and vice versa (Figure 4.11.2 (A-B)). The emission maxima also changed 8 nm in the whole region. The probable reason for the observation is that both hydrophobic and electrostatic interactions exist between the surfactant's positive and negative charge. Several unfold proteins wrap around the mixed micelle system. The most probable reason for the binding affinity is the strong synergism interaction among micelle solutions; they form aggregates in bulk solution, which disfavors the binding with protein.

All theoretical calculations have been carried out using the Gaussian16 quantum chemical package (details are provided in method section). The relative interaction energy (ΔE_{int}) (Figure 4.12 and Figure 4.13) is then calculated using the following relation: $\Delta E_{int} = E_{dimer} - E_{Sur1} - E_{Sur2}$, where E_{dimer} is the energy of the dimer coordinated with two surfactants and E_{Sur1} and

E_{Sur2} are the energy of two surfactant molecules, respectively. Interaction energy (ΔE_{int}) of two surfactants is evaluated to be -8.67 kJ/mol.

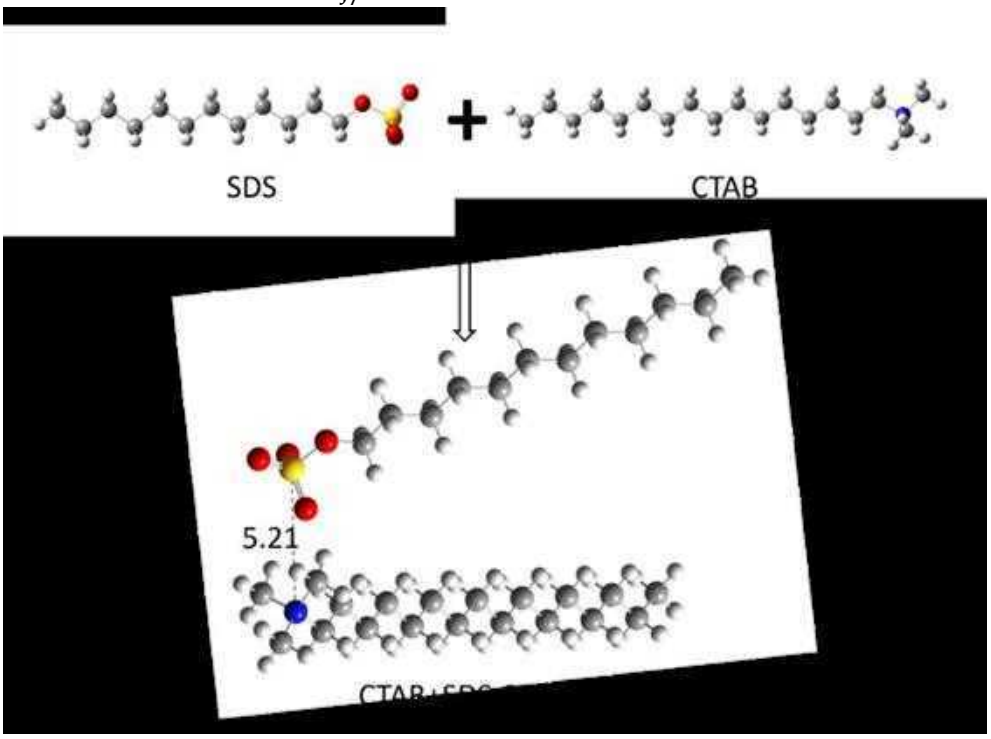


Figure 4.12 Optimized geometries of molecules: Color Code used in the figure: carbon(grey), oxygen (red), nitrogen (blue), hydrogen (white), Sulphur (yellow). Bond distances shown are in units of Å.

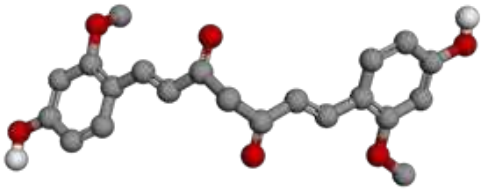


Figure 4.13 Energy minimized structure of Curcumin. Color code: carbon (grey), oxygen (red), hydrogen (white).

4.3.4 Heterogeneous Interaction between Curcumin and C102 in Live E.Coli observed by FRET Imaging

E. coli is a gram-negative bacteria and any molecular interaction of curcumin and other small molecules will be clearly understood by spectroscopic molecular ruler - FRET. Because of double layered structures of the *E. coli* membrane, the majority of molecules remain in the lipid membrane. Curcumin is hydrophobic and understanding of interaction of curcumin with small molecules will give a clear idea of nature of interactions with other molecules as well as bio-macromolecules and assemblies.

There is a significant spectral overlap between the fluorescence emission spectrum of C102 (donor) and the excitation absorption spectrum of curcumin (acceptor) which forms a good pair for studying FRET. Our goal is to study the interaction of curcumin in live bacteria cells. For that, we have taken 0.23 mM of C102 and 0.76 mM of curcumin solution and incubated with 2 million live *E. coli* cells which were grown as described in the experimental section. FRET is a non-radiative energy transfer process, and it is applied to calculate the efficiency (details in Experimental Section) between the C102 and curcumin in live *E. coli* (Figure 4.14).[146, 190, 213-214] To

visualize the spatial distribution of FRET efficiency in live E. coli, we used laser-scanning confocal microscopy, to image individual bacterial cells and resolve heterogeneities in membrane-associated molecular interactions

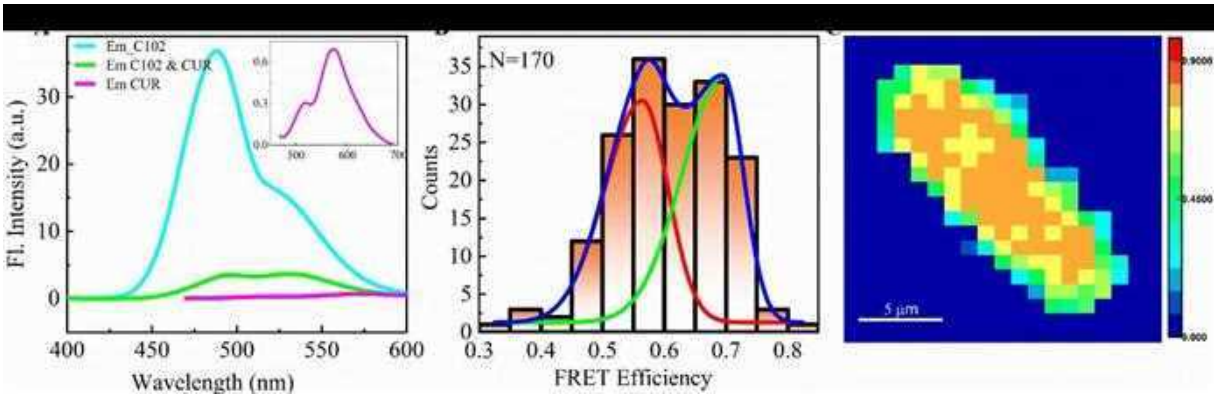


Figure 4.14 (A) Emission spectrum of only C102 (donor, cyan), only curcumin (acceptor, magenta) and in presence of both donor and acceptor (FRET condition) in water. Quenching of donor and rise of acceptor intensity in water are clearly indicated. Inset shows individual fluorescence of curcumin in absence of C102. (B) A histogram of FRET efficiency is calculated from 170 individual *E. coli* cells. Histogram shows heterogeneity in FRET efficiency, clearly indicating different patterns of interaction on live cell membrane. (C) A representative plot of FRET efficiencies in live bacteria cell membrane showing heterogeneity in molecular-level interactions.

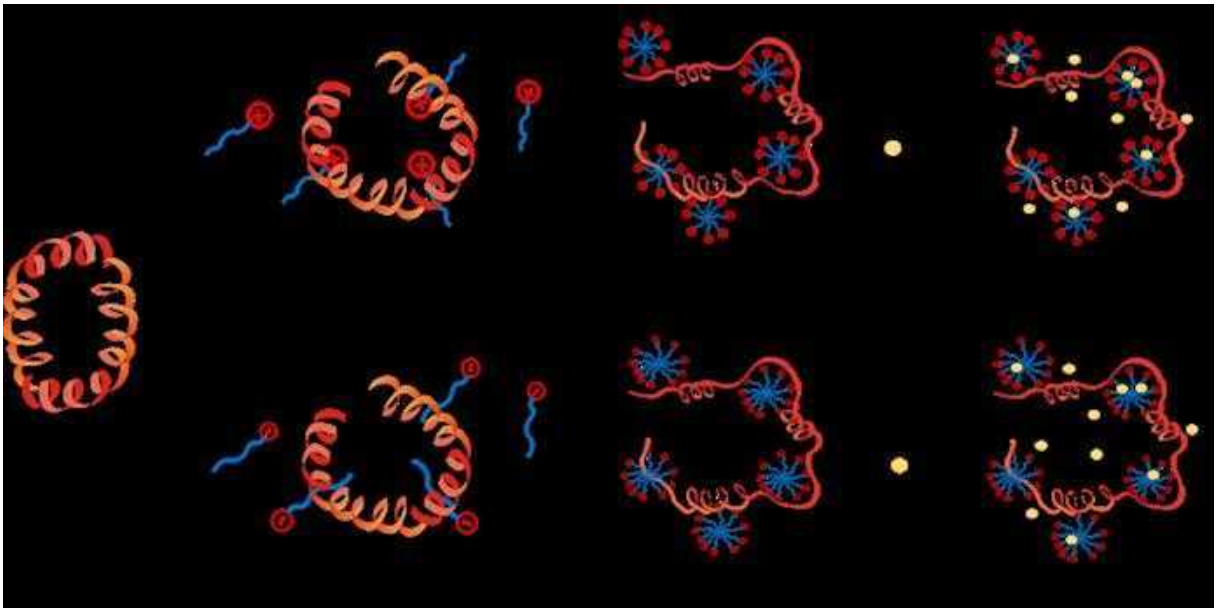
There are a few important observations. First, both dyes entered into bacteria membrane and have a significant interaction as calculated from the efficiency of FRET. As shown in Figure 4.14.B, there is a heterogeneity of FRET efficiency in the bacterial membrane – high FRET efficiency of 0.68 and low FRET efficiency of 0.56 after correction of bleed-through from donor to acceptor 3.3 % and 5.3% respectively. High FRET is possibly because of strong interaction of donor-acceptor inside core of double-layered gram-negative bacteria membrane, and low FRET efficiency is observed possibly because of presence of donor-acceptor inside the peptidoglycan wall in between outer and inner lipid membrane.[215] Heterogeneity in FRET efficiency clearly indicates different patterns of molecular interactions in cell membrane (Figure 4.14.C). Although curcumin is less soluble in bulk water, it can be well absorbed inside cell membrane and possibly inside the cells. Curcumin is hydrophobic and understanding of interaction of curcumin with small molecules will give a clear idea of nature of interactions with other molecules as well as bio-macromolecules and assemblies. This model can be used for development of curcumin delivery system in mammalian cells and tissue for further advanced studies.

The potential use of Curcumin as drug to cure many diseases are discussed before and there are many ongoing clinical trials. However, the lack of solubility is a main challenge. The model delivery system of protein/curcumin/surfactants can be a potential solution as curcumin is not replaced by surfactants in competitive binding. Similar lipid delivery system is reported before. The interaction of small molecules is studied here by FRET imaging in E.coli, and it will give a potential idea how curcumin may be delivered in live mammalian cells or tissues.
Figure 4.1 shows blue shift of emission spectra of Tryptophan in BSA in presence of surfactants. To interpret the data, we proposed a model (Scheme 1) that partially unfolded protein specifically Tryptophan locations of protein may either go through hydrophobic core of micelle or protein itself may form a coil around the ionic micelle due to electrostatic interactions.

Recently, J. Pedersen et al.[181] reported that an initial process of aggregate formation of protein and SDS is rapid, which is followed by two slower processes, where the complexes first disaggregated into single protein structures situated asymmetrically on the SDS micelles, followed by isotropic redistribution of the protein. This report of coiling around micelle structure

was supported by blue-shift emission spectra, CD and SAXS data. In addition, N. J Turro et al. reported two possible "necklace and bead structures" of protein-surfactant interaction complexes - (1) protein recoils around the micelles, and thus mobility of the surfactant head group is significantly decreased, and (2) the micelles nucleate at hydrophobic sites of protein, and the mobility of the surfactant head groups is not changed much. This report was supported by fluorescence spectroscopy.[20]

In our proposed model, we reported that depending on the charge of the surfactant head group, it interacts differently with negatively charged BSA, particularly below the critical micelle concentration (CMC). As shown in Scheme 1, the positively charged head group of CTAB interacts directly with the negatively charged BSA through electrostatic attraction, whereas the negatively charged SDS head group is repelled by BSA's similar charge, resulting in interaction primarily via the surfactant's hydrophobic tail. This differential interaction behavior has also been noted in earlier studies on protein–surfactant binding mechanisms.[209] Above the CMC, the partially unfolded protein chain interacts (1) directly with hydrophobic micelles, sometimes embedding Trp residues within the micelle core, and (2) wraps around the micelle depending on the surfactant head group's charge and the position of oppositely charged amino acids in the protein backbone.



Scheme 4.1. Schematic representation of the interaction of native BSA with cationic (CTAB) and anionic (SDS) surfactant effecting partially unfolding below and above CMC. Curcumin loading is shown at the hydrophobic core of micelle and protein.

Table 4.1 Thermodynamic Parameters and Quenching Constants of BSA + SDS & BSA + CTAB Assemblies.

Surfactant	Regions	Quenching constant (K_{sv}) ± SE (L mol^{-1})	Binding Constants (K) ± SE (M^{-1})	Number of binding sites ± SE (n)
BSA + SDS	Region A (0.2-0.4 mM)	(0.55±0.13) × 10^3	2.09±0.13	2.48±0.13

	Region B (0.5-10 mM)	$(0.07\pm0.08) \times 10^3$	2.86±0.07	0.57±0.07
	Region C (15-40 mM)	$(0.02\pm0.13) \times 10^3$	2.38±0.01	0.17±0.01
BSA + CTAB	Region A (>0.3 mM)	$(0.94\pm0.06) \times 10^3$	2.64±0.5	2.41±0.5
	Region B (0.4-5 mM)	$(0.20\pm0.28) \times 10^3$	2.19±0.11	0.68±0.11
	Region C (5-40 mM)	$(0.009\pm0.06) \times 10^3$	2.36±0.15	0.07±0.15

Table 4.2 Thermodynamic Parameters and Quenching Constants of BSA + Curcumin & BSA + SDS + Curcumin Assemblies.

	Quenching Constant (K_{sv}) ± SE (L mol^{-1})	**Binding constant (K) ± SE (M^{-1})**	**Number of Binding Sites± SE (n)**
BSA + Curcumin	$(8.16\pm0.98) \times 10^3$	2.87±0.13	0.54±0.13
BSA + Curcumin + SDS	$(0.012\pm0.03) \times 10^3$	2.94±0.10	0.284±0.10

Table 4.3 Molecular Docking Result Analysis.

Hydrophobic Interaction Between BSA and curcumin			**The hydrogen bond between amino acid and curcumin**		
Amino Acid	**Residue**	**Distance (Å)**	**Amino Acid**	**Residue**	**Distance (Å)**
ARG	208 A	3.63	LYS	211A	3.37
LYS	211A	3.43	LEU	480A	2
LEU	346A	3.75			
ALA	349A	3.76			
VAL	481A	3.45			

4.4 Conclusion

In conclusion, we report the utilization of protein and micelle systems for efficient delivery of curcumin which has low solubility in water by applying fluorescence spectroscopy and confocal imaging. Both cationic and anionic micelle causes blue shift of emission maxima of native protein, which unfolds in the presence of surfactant above CMC. In addition, the enhanced binding constants are also attributed towards the incorporation of tryptophan residues inside the

hydrophobic core of micelle, and blue-shifted emission is observed even in denatured protein system (Scheme 1). The curcumin drug not only incorporates inside the hydrophobic core of micelle but also at hydrophobic core of protein, and thus making the combined system a better drug delivery carrier (Scheme 4.1). Although there are many ongoing clinical trials to develop curcumin as a natural drug, actual challenges are solubility in water and efficient delivery at physiological conditions. Future research could concentrate on the direct examination of curcumin administration to E. coli cells utilizing BSA or micelle-based carrier systems. Although our current investigation carefully investigates curcumin's interaction with BSA and surfactants and independently verify its placement on the bacterial membrane, these components were not employed in a combined delivery experiment. Conducting research that incorporates the pre-loading of curcumin into protein-micelle complexes and monitoring their cellular absorption in E. coli or mammalian systems will be essential for addressing this gap. Our understanding of the molecular mechanism of the interaction of curcumin with protein and micelle in water and cell membrane may shed light on the development of efficient curcumin delivery towards the goal of applying curcumin as a natural drug against life-threatening diseases.